Large volume collapse observed in the phase transition in cubic PbCrO$_3$ perovskite

Wansheng Xiao[a], Dayong Tan[a], Xiaolin Xiong[a], Jing Liu[b], and Jian Xu[c,d,1]

[a]Guangzhou Institute of Geochemistry, Chinese Academy of Sciences, Guangzhou 510640, China; [b]Institute of High Energy Physics, Chinese Academy of Sciences, Beijing 100049, China; [c]Institute of Fluid Physics, China Academy of Engineering Physics, Mianyang 621900, China; and [d]Institute of Atomic & Molecular Physics, Sichuan University, Chengdu, 610065, China

When cubic PbCrO$_3$ perovskite (Phase I) is squeezed up to ∼1.6 GPa at room temperature, a previously undetected phase (Phase II) has been observed with a 9.8% volume collapse. Because the structure of Phase II can also be indexed into a cubic perovskite as Phase I, the transition between Phases I and II is a cubic to cubic isostructural transition. Such a transition appears independent of the raw materials and synthesizing methods used for the cubic PbCrO$_3$ perovskite sample. In contrast to the high-pressure isostructural electronic transition that appears in Ce and SmS, this transition seems not related with any change of electronic state, but it could be possibly related on the abnormally large volume and compressibility of the PbCrO$_3$ Phase I. The physical mechanism behind this transition and the structural and electronic/magnetic properties of the condensed phases are the interesting issues for future studies.

high pressure | X-ray diffraction | DAC | electron state

Phase transitions are one of the most fundamental research topics in physics, chemistry, bioscience, and geosciences. Ordinarily, an isostructural phase transition is accomplished with a volume collapse without any symmetrical change. For example, a 6.6% volume change at ∼105 GPa appears during the transition of the B8 structure of MnO due to the Mott transition (1), a 2% volume change at 5.5 GPa occurs in the transition of hexagonal to the same structure ThAl$_2$ (2), and a 4.0–6.5% volume change appears in the transition of the orthorhombic perovskites of PrFeO$_3$, EuFeO$_3$, and LuFeO$_3$ to also orthorhombic structure around 50 GPa (where the transition is considered a high-spin to low-spin transition of the Fe ions) (3). In these transitions, although their axial ratios of both a/c and b/c change with their volume at various pressures, the atomic symmetric does not change. In fact, the isostructural phase transitions induced by high pressures are rare and special transitions usually considered to be originating from the electronic structural change in the matter; such a transition appears in cubic Ce (γ-α) and SmS (B1) (4, 5) at room temperature at 0.7 GPa and 0.65 GPa with volume reductions of 15.0% and 13.6%, respectively. Recent evidence suggests that a transition in Ce occurs when the localized f-electron in this system becomes delocalized. Therefore, this transition has been contemporarily referred to as a kind of electronic transition. The volume collapse is therefore considered as a Kondo volume collapse (6). A similar transition appears in Cs, that is, from a face-centered cubic (fcc) phase II to fcc Phase III. It has also been considered as an electronic fcc isostructural transition from 6s to 5d, with a ∼9% volume reduction at around 4.2 GPa (7–9), although recent work has shown that the detailed structure of Phase III is no longer fcc but exactly belongs to a complex large monoclinic ($C222_1$) lattice with 84 atoms (10).

Transition-metal oxides with ABO$_3$ perovskite structure show special properties, such as ferro-electricity, ferro-magnetism, ferro-elasticity, multiferroic, giant magneto-resistive (GMR). They are initiated from the interaction among the orbit spin of 3d electrons of the transition metallic B ion in the BO$_6$ octahedral. In addition, the stereo chemical characters of the A ion with lone pair electrons also play an important role. Although a this kind of

ACr^{4+}O$_3$ perovskite (CaCrO$_3$, SrCrO$_3$, PbCrO$_3$) has been synthesized as quickly as 60 s (11–16), interesting progress has been made in recent investigations (17–25). On the research of the low temperature structure and electric/magnetic properties of CaCrO$_3$ and SrCrO$_3$, the ordering of the orbital in the 3d^2 electrons of Cr^{4+} ion has been observed, and it makes a structural distortion (18, 19) or even a transition from a cubic to a tetragonal (18).

Normally, the PbCrO$_3$ cubic perovskite can be synthesized through a high-pressure and high-temperature process carried out either by the mixture of PbO and CrO$_2$ powder (15) or by the decomposition from PbCrO$_4$ powder.

$$PbO + CrO_2 \rightarrow PbCrO_3 \qquad [1]$$

and

$$2PbCrO_4 \rightarrow 2PbCrO_3 + O_2. \qquad [2]$$
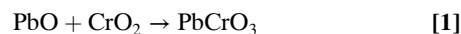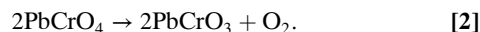
These synthesizing conditions have been determined at about 5.5–7.0 GPa and 1,000–1,700 K as reported by DeVries and Roth (15). More recently, it has been also synthesized at 8 GPa and 1073 K by Arévalo-López and Alario-Franco (23). Under ambient conditions, this PbCrO$_3$ cubic perovskite (labeled as Phase I below) is a black powder with a lattice constant of 4.0132(4) Å that is in good agreement with the previously reported data of about 4.00 Å determined by X-ray diffraction on single crystal and powder samples and powder neutron diffraction (14–16). This phase has been, furthermore, considered as actually formed by a compositionally modulated $a_p \times 3a_p \times (14 \sim 18)a_p$ superlattice structure, where $a_p = 4.002(1)$ Å is the lattice constant of the cubic PbCrO$_3$ perovskite (23), and the broadened X-ray diffraction peaks of Phase I, even when only the X-ray $K_{\alpha 1}$ radiation is used in the diffraction experiments (16, 23), was considered to be as a result of complex structure (23–25). PbCrO$_3$ Phase I is a semiconductor with a resistance of 2.6×10^3 $\Omega \cdot$ cm (16), which agrees well with the recent result of resistance determination between 210 K and 395 K (25). Because of the existence of unpaired electrons, each Cr ion has an atomic spin magnetic moment ∼1.9 μ_B (16) or 2.51 μ_B (25), which makes the Phase I a G-type antiferromagnetic semiconductor (16, 25). The Neel temperature has been reported to range from 245 K to 160 K (according to different measurements) (14, 16, 25). From the temperature relationship of electrical resistance, the activation energy of the Phase I perovskite was calculated to be 0.27 eV (16), or 0.27 ev and 0.11 ev in different temperature ranges (25). An anomalous change appears in the temperature relationships describing resistance and susceptibility in the 100 K range (16).

GEOLOGY

The volume of $PbCrO_3$ phase I seems to be somewhat abnormally large. From the point of view of the atomic sphere approximation, the lattice constants of ABO_3-type perovskites mostly depend on their A- and B-atomic radii; however, the ~4.00 Å lattice constant of cubic $PbCrO_3$ perovskite Phase I is much larger than that of $SrCrO_3$ (3.82 Å) [17] and $PbTiO_3$ (3.96 Å) (ICDD 40-0099) but is similar to $BaRuO_3$ (4.006 Å) [26], although the atomic radii of Sr (1.44 Å), Ti (0.605 Å), Ba (1.61 Å), and Ru (0.62 Å) are either similar to or larger than that of Pb (1.49 Å) and Cr (0.55 Å), respectively [27]. Comparing the ion radius of V^{4+} (0.58 Å) [27] with that of Cr^{4+}, the volume of $PbCrO_3$ cubic perovskite Phase I is much larger than that of the cubic perovskite $PbVO_3$ ($a \sim 3.9$ Å) existing above 2 GPa [28], which also reflects the unusual structure of $PbCrO_3$ Phase I at ambient conditions, although it is a little smaller than that of the strongly distorted tetragonal perovskite $PbVO_3$ ($c/a = 1.23$) [28]. Here, we report on a unique isostructural transition that produces a previously undescribed, high-pressure cubic $PbCrO_3$ perovskite phase (Phase II). At room temperature and ~1.6 GPa, a 9.8% volume change from Phase I to Phase II has been observed.

Results and Discussion

A typical in situ angle dispersive X-ray diffraction (ADXD) pattern and the diffraction intensity distribution of the cubic $PbCrO_3$ perovskite are shown in Fig. 1, which depicts the data for Phase II taken at 20.3 GPa [where most of the peaks can be compared with the expected results for a cubic perovskite with a lattice constant of 3.7408(5) Å]. In addition, except for the diffraction peaks of the pressure medium (Ar), a small number of peaks from impurities can also be seen, with varying positions depending on the raw materials used. The spotty perovskite peaks

indicate that overheating occurred during our laser heating process. As a result, the spottiest pattern in our measurements has been shown in Fig. 1. Actually, such a special sample received an additional 1,900 K to 2,100 K laser heating in the 16IDB beam line at High Pressure Collaborative Access Team, Advanced Photon Source, Argonne National Laboratory, Argonne, IL. Good agreement is observed among all synthesized $PbCrO_3$ cubic perovskite on their ADXD patterns obtained from different X-ray sources and the samples as well as in the pressure increasing/decreasing sequences. The standard deviations determined from all of the diffraction peaks indexed as two cubic perovskites are small; they indicated that the distortions in these cubic phases are small. The zero-pressure lattice constant (4.0132 Å) of $PbCrO_3$ Phase I in this study is in good agreement with reported experimental values [14–16, 23].

The phase transition process between the two kinds of cubic perovskites is shown in Fig. 2, in which the starting material is $PbCrO_4$ and X-ray wavelength is 0.6202 Å. The diffraction pattern at 1.6 GPa shows the coexistence of two cubic $PbCrO_3$ perovskite phases, and these two phases are stable in their own pressure regions. The two sets of diffraction lines of $PbCrO_3$ at 1.6 GPa pattern can be indexed as two cubic perovskite structures with the lattice constant of $a = 3.9789(7)$ Å and volume of $V = 62.99(3)$ Å^3 for the low-pressure phase (Phase I) and $a = 3.8443(4)$ Å and $V = 56.81(2)$ Å^3 for the high-pressure phase (Phase II). The pair sets of the indexed peaks and the diffracted spotty character of both phases also demonstrate clearly the cubic-to-cubic transition. The volume difference up to 9.8% between them in the coexisting pattern indicates a first order phase transition. The cubic-to-cubic transition process is also observed at another experimental run in which the mixture of $PbO + CrO_2$ is used as raw material. Actually, the phase transition

Fig. 1. A typical X-ray diffraction image of the cubic $PbCrO_3$ perovskite at 20.3 GPa. Most of the peaks can be identified as cubic perovskite (Phase II) with a lattice constant of 3.7408 Å. In addition, except for the peaks associated with the pressure medium (Ar), the peaks from various impurities are still detectable. These peaks are different when different raw materials are used.

Fig. 2. Several X-ray diffraction images of the cubic $PbCrO_3$ perovskite at various pressures. A cubic-to-cubic transition between Phase I and Phase II can be seen at ~1.6 GPa. Two sets of diffraction peaks are depicted.

between Phase I and Phase II is reversible. All of the Phase I material in either of our experimental runs or of references were obtained from the decompressed Phase II. We have not found any residual Phase II in both of the initial Phase I and the Phase I in the DAC after the pressure released.

The equations of states (EOSs) were determined for the two cubic $PbCrO_3$ perovskites. The measured pressure-volume data from all five experimental runs for both phases are shown in Fig. 3. Fitting the two sets of P-V data of both phases into the Birch–Murnaghan EOS with a fixed bulk modulus pressure derivative, K_0', as 4 yields the EOS parameters of the bulk modulus, K_0, of 59(5) GPa and the volume, V_0, of 64.64(7) $Å^3$ for the Phase I, K_0 of 187(4) GPa and V_0 of 57.61(8) $Å^3$ for the Phase II, respectively. The bulk modulus of Phase II is comparable to that of $CaCrO_3$ and $SrCrO_3$ perovskites (17); however, $K_0 = 59$ GPa of Phase I, which is about one-third of the experimental values of $CaCrO_3$, $SrCrO_3$ and the high-pressure cubic $PbCrO_3$ perovskite, is indeed too small for an oxide perovskite.

Isostructural phase transitions with large volume collapses are rare. Such transitions are normally related to a change of electronic state, as in the cases of Ce and SmS. In the case of $PbCrO_3$, on the one hand, the $3d^2$ valence electrons in the Cr^{4+} ion occupy the t_{2g} orbit in the $CrO_{6/2}$ coordinated octahedron, which is a kind of electronic combination of weak Jahn–Teller effect. Because of such a combination, the high-spin to low-spin transitions are not easily turned on. On the other hand, the valence electrons of Pb^{2+} ion are the $6s^2$ single lone pair electrons. With such a configuration it seems impossible to produce a transition from $6s$ to $6p$ at low pressures. Therefore, the pressure induced cubic-to-cubic transition of $PbCrO_3$ perovskite seems improbable due to the transition between these states of electrons.

The distortion from a standard perovskite structure depends upon the mismatch between the radii of the A ion and B ion. A geometrical tolerance factor t, $t = (r_A + r_X)/\sqrt{2}(r_B + r_X)$ (where r_A and r_B are the radii of the A and B cations, respectively, and r_X is the radius of the anion) was proposed to monitor this mismatch. Using the ion radii (27), the tolerance factor t of the $PbCrO_3$ is 1.057, which is slightly beyond the suitable range of a cubic

perovskite. Although the particular ion-radii values used in the relationship were not correct (due to the fact that the coordinated numbers were ignored in the authors' original data analysis) (29), an empirical relation used to predict the lattice constants of possible cubic perovskite structure through the ion radius gives a good prediction based on summarizing 132 kinds of cubic or pseudocubic perovskite (30). Ubic (31) suggested the improved formula,

$$a_{calc} = 0.06741 + 0.490523(r_A + r_X) + 1.29212(r_B + r_X).$$

Under ambient conditions, the extrapolated zero-pressure lattice constant of the high-pressure cubic $PbCrO_3$ perovskite (Phase II) of 3.862 Å agrees well with the empirical relationship (3.857 Å, with a deviation of 0.18%), whereas the lattice constant (4.013 Å) of the low-pressure phase (Phase I) is far beyond that of the formula. The deviation (3.88%) from the formula is also much larger than the average deviation (0.60%) for these kinds of cubic perovskites and is more than twice the third deviation of 1.86% ($CaVO_3$).

To date, no successful first principle calculations have been carried out for cubic $PbCrO_3$ perovskites, although earlier Linear Muffin-Tin Orbital (LMTO) calculations have predicted the correct magnetic moment of the Cr ions. However, this calculation has not been able to predict a correct electronic band gap (32). Our preliminary first principle calculations predict an equilibrium lattice constant of 3.775 Å from LDA and 3.847 Å from GGA with a bulk modulus of 230 GPa and 192 GPa, respectively, for the cubic $PbCrO_3$ perovskite at ambient conditions. The GGA results agree well with the corresponding values of the high-pressure cubic $PbCrO_3$ perovskite (Phase II) observed in this study but are far away from the experimentally observed values of ~4.00 Å and 59 GPa in Phase I. In addition, in the cubic symmetrical frame, the additional on-site repulsion term U did not help to predict the structural properties of Phase I. These experimental and theoretical evidences indicate that a new structural and electronic description is required to model the properties of $PbCrO_3$ Phase I. As described earlier, $3d$ orbital ordering in the $CrO_{6/2}$ octahedron is used to explain the structural distortion of $CaCrO_3$ and $SrCrO_3$ perovskite without obvious volume change (18, 19). These phase transitions are different from those with the large volume collapse in $PbCrO_3$. The spin reorientation is also considered to play an important role in the structure and complex properties of the $PbCrO_3$ Phase I (25). However, the added spin terms have not improved our first principle calculations. Alternately, if the $CrO_{6/2}$ replaced by $PbO_{6/2}$ octahedron in the cubic perovskite structure, our first principle calculations result in a lattice constant of 4.136 Å for LDA and 4.214 Å for GGA, respectively. The real Phase I might be a kind of mixture of random $PbCrO_3$-$CrPbO_3$ combination, which results in a cubic perovskite diffraction pattern with a lattice constant of about 4.00 Å. Possibly, it might be disorderly interpenetrating simple cubic structure of each Cr and Pb (similar to the B2 structure) with the weak diffraction of the oxygen atoms.

In conclusion, we have synthesized the cubic $PbCrO_3$ perovskite by using different raw materials and synthesizing methods at high-pressure/high-temperature conditions in DAC successfully. Experiments reveal that the cubic $PbCrO_3$ perovskite Phase I is transferring into a cubic perovskite Phase II at about 1.6 GPa with a large (9.8%) volume collapse in the first time. The structural properties of Phase II agree well with both empirical prediction and first principle calculations. However, Phase I shows abnormal large volume and compressibility. The real Phase I might be a kind of mixture of $PbCrO_3$-$CrPbO_3$ combination, although more detailed study is needed.
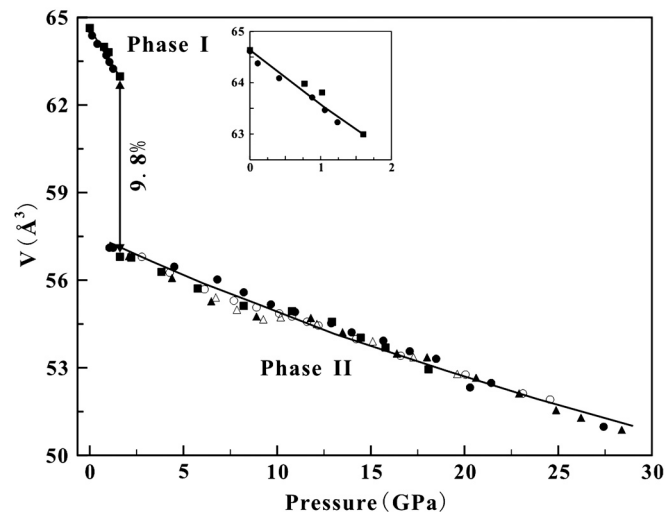

Fig. 3. The equation of state (EOS) of the cubic $PbCrO_3$ perovskites. A volume collapse of 9.8% occurs at about 1.2–1.6 GPa, which is the location where the phase transition occurs between Phases I and II. The small inset plot refers to the P-V relation for Phase I. The scattered data in all of five experimental runs results in a large fitting error into the fitted parameters of the Birch–Murnaghan equation. In this plot, the circle indicates the raw materials by used PbO + CrO_2 (solid: pressure release process; empty: pressure increase process); the other three signals indicate that the experimental sample was made from raw $PbCrO_4$, and all of the points were taken in the pressure release process.

GEOLOGY

Materials and Methods

The PbCrO$_3$ cubic perovskite samples used in this study were synthesized in Mao-Bell-type DAC. Two kinds of raw materials were used for the two aforementioned reaction processes. In the first process, yellow PbO powder (Alfa Aesar), which has a *Pcam* structure with lattice constants *a*, *b*, and *c* that are equal to 5.5041 Å, 5.5095 Å, and 4.7635 Å, respectively, and black CrO$_2$ powder (Sigma-Aldrich), which has a rutile-like *P4$_2$/mnm* structure with lattice constants *a* and *c* that are equal to 4.4218 Å and 2.9172 Å, respectively, were stoichiometrically mixed and ground together. In the second process, chemical reagent grade PbCrO$_4$ (produced by Guangdong Chemical Reagent Engineering, Technological Research and Development Center), which has a *P2$_1$/n* structure with lattice constants *a*, *b*, *c*, and β that are 7.1262 Å, 7.4332 Å, 6.7967 Å, and 102.45°, respectively, was used.

Small disks of the aforementioned two kinds of raw materials were pressed and loaded into the sample hole in the T301 stainless steel gasket (indented to ~40 µm from an original thickness of 250 µm) of the DAC with Ar as the pressure medium and as the insulator during laser heating. The samples in the DAC were squeezed up to 18–30 GPa and then heated by YAG laser at the Guangzhou Institute of Geochemistry to temperatures of around 1,200 to 1,500 K. Using these samples with different sequences in which the pressure was increased or decreased, a total of five in situ ADXD experimental runs were carried out in the 4W2 beam line at BSRF (Beijing Synchrotron Radiation Facility) using a 0.6202 Å X-ray beam and Mar345 detector, as well as with a monochromic 0.6176 Å X-ray beam and classic off-line image plate in the BL-18C beam line at KEK (High Energy Accelerator Research Organization, Japan). Runs were also carried out in the 16IDB beam line (High Pressure Collaborative Access Team, Argonne National Laboratory, Argonne, IL) using either a 0.3680 or 0.4666 Å X-ray beam and MarCCD detector. The collected diffraction patterns were analyzed by intergrating images as a function of 2θ

using the program either Fit2D (33) or WinPIP to obtain a conventional, one dimensional diffraction profile. The pressures in all of the experiments were determined by the ruby scale (34).

The preliminary first principle calculation for the cubic PbCrO$_3$ perovskite for Pb 5d^{10} 6s^2 6p^2, Cr 3s^2 3p^6 3d^5 4s^1 and O 2s^2 2p^4 was performed by CASTEP program (35) in Materials Studio package with the geometry optimization. The energy cut-off of 1000 ev and the ultrasoft pseudopotential were chosen in the calculations. As for the Brillouin zone k-point sampling, we have used the $6 \times 6 \times 6$ Monkhorst–Pack scheme. In the process, at various pressures, both exchange correlation functionals of LDA with CA-PZ and GGA with PBE were used to optimize the lattice parameter for the cubic symmetry and furthermore the zero bulk modulus was obtained by fitting the P-V data into the third order Birch-Murnaghan equation. The similar process was done on the possible cubic CrPbO$_3$ perovskite with a simple location switching between Pb and Cr ions in the basic cubic PbCrO$_3$ perovskite frame.

1. Yoo CS, et al. (2005) First-order isostructural Mott transition in highly compressed MnO. *Phys Rev Lett* 94:115502.
2. Shekar NVC, Sahu PCh, Sekar M, Yousuf M, Rajan KG (1996) Pressure induced isostructural and structural transitions in ThAl$_2$. *Physica B* 228:369–373.
3. Rozenberg GK, et al. (2005) Consequences of pressure-instigated spin crossover in RFeO$_3$ perovskites; a volume collapse with no symmetry modification. *Europhys Lett* 71:228–234.
4. Hall HT, Merrill L, Barnett JD (1964) High pressure polymorphism in Cesium. *Science* 146:1297–1299.
5. Maple MB, Wohlleben D (1971) Nonmagnetic 4*f* shell in the high-pressure phase of SmS. *Phys Rev Lett* 27:511–515.
6. Lipp MJ, et al. (2008) Thermal signatures of the Kondo volume collapse in cerium. *Phys Rev Lett* 101:165703.
7. Lawson AW, Tang TY (1949) Concerning the high pressure allotropic modification of cerium. *Phys Rev* 76:301–302.
8. Louie SG, Cohen ML (1974) Electronic structure of cesium under pressure. *Phys Rev B* 10:3237–3245.
9. Abd-Elmeguid MM (1995) ^{133}Cs high pressure Mössbauer spectroscopy: A new powerful tool for studying charge transfer and lattice dynamics in metallic Cs. *Hyperfine Interact* 95:265–275.
10. McMahon MI, Nelmes RJ, Rekhi S (2001) Complex crystal structure of Cesium-III. *Phys Rev Lett* 87:255502.
11. Chamberland BL (1967) Preparation and properties of SrCrO$_3$. *Solid State Commun* 5:663–666.
12. Goodenough JB, Longo JM, Kaflas JA (1968) Band antiferromagnetism and new perovskite CaCrO$_3$. *Mater Res Bull* 3:471–482.
13. Weiher JF, Chamberland BL, Gillson JL (1971) Magnetic and electrical transport properties of CaCrO$_3$. *J Solid State Chem* 3:529–532.
14. Roth WL, DeVries RC (1967) Crystal and magnetic structure of PbCrO$_3$. *J Appl Phys* 38:951–952.
15. DeVries RC, Roth WL (1968) High-pressure synthesis of PbCrO$_3$. *J Am Ceram Soc* 51:72–75.
16. Chamberland BL, Moeller CW (1972) A study on the PbCrO$_3$ perovskite. *J Solid State Chem* 5:39–41.
17. Zhou J-S, Jin C-Q, Long YW, Yang LX, Goodenough JB (2006) Anomalous Electronic State in CaCrO$_3$ and SrCrO$_3$. *Phys Rev Lett* 96:046408.
18. Ortega-San-Martin L, et al. (2007) Microstrain sensitivity of orbital and electronic phase separation in SrCrO$_3$. *Phys Rev Lett* 99:255701.
19. Komarek AC, et al. (2008) CaCrO$_3$: An anomalous antiferromagnetic metallic oxide. *Phys Rev Lett* 101:167204.
20. Streltsov SV, Korotin MA, Anisimov VI, Khomskii DI (2008) Band versus localized electron magnetism in CaCrO$_3$. *Phys Rev B* 78:054425.
21. Castillo-Martínez E, Durán A, Alario-Franco MÁ (2008) Structure, microstructure and magnetic properties of Sr$_{1-x}$Ca$_x$CrO$_3$ ($0 \leq x \leq 1$). *J Solid State Chem* 181:895–904.
22. Castillo-Martínez E, Arévalo-López AM, Ruiz-Bustos R, Alario-Franco MA (2008) Increasing the structural complexity of chromium(IV) oxides by high-pressure and high-temperature reactions of CrO$_2$. *Inorg Chem* 47:8526–8542.
23. Arévalo-López ÁM, Alario-Franco MÁ (2007) On the structure and microstructure of "PbCrO$_3$". *J Solid State Chem* 180:3271–3279.
24. Arévalo-López ÁM, Castillo-Martínez E, Alario-Franco MÁ (2008) Electron energy loss spectroscopy in ACrO$_3$ (A = Ca, Sr and Pb) perovskites. *J Phys-Condens Mat* 20:505207.
25. Arévalo-López ÁM, santos-Garcia AJD, Alario-Franco MÁ (2009) Antiferromagnetism and spin reorientation in "PbCrO$_3$". *Inorg Chem* 48:5434–5438.
26. Jin C-Q, et al. (2008) High-pressure synthesis of the cubic perovskite BaRuO$_3$ and evolution of ferromagnetism in ARuO$_3$ (A = Ca, Sr, Ba) ruthenates. *Proc Natl Acad Sci USA* 105:7115–7119.
27. Shannon RD (1976) Revised effective ionic radii and systematic studies of interatomic distances in halides and chalcogenides. *Acta Crystallogr A* 32:751–767.
28. Belik AA, Azuma M, Saito T, Shimakawa Y, Takano M (2005) Crystallographic features and tetragonal phase stability of PbVO$_3$, a new member of PbTiO$_3$ family. *Chem Mater* 17:269–273.
29. Moreira RL, Dias A (2007) Comment on "Prediction of lattice constant in cubic perovskites". *J Phys Chem Solids* 68:1617–1622.
30. Jiang LQ, et al. (2006) Prediction of lattice constant in cubic perovskites. *J Phys Chem Solids* 67:1531–1536.
31. Ubic R (2007) Revised method for the prediction of lattice constants in cubic and pseudocubic perovskites. *J Am Ceram Soc* 90:3326–3330.
32. Jaya SM, Jagadish R, Rao RS, Asokamani R (1992) Electronic structure of the perovskite oxides SrCrO$_3$ and PbCrO$_3$. *Mod Phys Lett B* 6:103–112.
33. Hammersley AP, Svensson SO, Hanfland M, Fitch AN, Hausermann D (1996) Two-dimensional detector software: From real detector to idealised image or two-theta scan. *High Pressure Res* 14:235–248.
34. Mao HK, Xu J, Bell PM (1986) Calibration of the ruby pressure gauge to 800 kbar under quasi-hydrostatic conditions. *J Geophys Res* 91:4673–4676.
35. Segall MD, et al. (2002) First-principles simulation: ideas, illustrations and the CASTEP code. *J Phys-Condens Mat* 14:2717–2743.